Journal of Power Sources 265 (2014) 345–355

Contents lists available at ScienceDirect

Journal of Power Sources

journal homepage: www.elsevier.com/locate/jpowsour

New bio-polymeric membranes composed of alginate-carrageenan to be applied as polymer electrolyte membranes for DMFC

S.D. Pasini Cabello [a], S. Mollá [b], N.A. Ochoa [a], J. Marchese [a], E. Giménez [c], V. Compañ [b,*]

[a] Instituto de Física Aplicada (INFAP), Universidad Nacional de San Luis CONICET, Chacabuco 917 5700 San Luis, Argentina
[b] Departamento de Termodinámica Aplicada, Universidad Politécnica de Valencia, 46022 Valencia, Spain
[c] Departamento de Ingeniería Mecánica y de Materiales, Universidad Politécnica de Valencia, 46022 Valencia, Spain

HIGHLIGHTS

- Membranes of alginate with κ-carrageenan have been studied for DMFC application.
- Proton conductivity and methanol permeability increase with the carrageenan content.
- Carrageenan diminishes the stability of the membranes above a 20 wt% content.
- Large increase of the static permittivity at 20 wt% Car is explained by percolation.

ARTICLE INFO

Article history:
Received 20 January 2014
Received in revised form
7 April 2014
Accepted 18 April 2014
Available online 29 April 2014

Keywords:
Bio-polymeric membranes
Polymer electrolyte membrane
Conductivity
Methanol permeability
DMFC

ABSTRACT

Novel polyelectrolyte membranes were prepared from pure solutions of alginate (Alg), carrageenan (Car) and their mixtures. The films were crosslinked and sulfonated and then, characterized by several techniques: ionic exchange capacity (IEC), water uptake, mechanical thermal properties, and also functional properties such as methanol permeability and proton conductivity. The results show that Alg/Car membranes have a ductile behavior. Low carrageenan concentrations have a weak thermoprotective effect, which slightly delays both T_g and T_m of prepared membranes. The methanol permeability of Alg/Car membranes increase with the carrageenan content varying from 0.55×10^{-6} cm^2 s^{-1} for Alg/Car 100/00 to 4.89×10^{-6} cm^2 s^{-1} for Alg/Car 80/20. The Proton conductivities of the membranes increase with the carrageenan content from 9.79×10^{-3} S cm^{-1} for Alg/Car 100/00 until 3.16×10^{-2} S cm^{-1} for Alg/Car 80/20 at 90 °C. Finally the proton transfer mechanism is discussed in terms of the conductivity activation energy and the dependence of the proton diffusion coefficient with the temperature has been studied.
© 2014 Elsevier B.V. All rights reserved.

1. Introduction

With the worldwide increasing demand for clean and sustainable energy, fuel cells have been touted as an environmentally friendly and efficient substitute of conventional fossil fuel power sources. Direct methanol fuel cells (DMFCs) are considered to be one of the most promising candidates for transportation, distributed power, and portable power applications, but important scientific, technical and economic problems need to be solved before commercialization is possible. The interest in membranes arises in part from the potential use of these materials as electrolytes in low temperature fuel cells [1,2]. The core part of a DMFC is the proton exchange membrane (PEM), which facilitates proton transport between electrodes and separates the fuel from the oxidant. Nafion® (a perfluorosulfonic acid copolymer), as the current state-of-the-art PEM material, shows excellent chemical and mechanical stability along with high proton conductivity at moderate operation temperatures (≤80 °C) and high relative humidity [3,4]. However, Nafion®-type membranes have serious drawbacks such as high production cost, reduced proton conductivity above 80 °C, and high methanol crossover. These disadvantages have limited their widespread commercial applications, especially for the DMFCs [5,6]. Therefore, research on alternative polymer electrolyte membranes with low cost and high conductivity has been stimulated. The synthesis of cation-exchange membranes that combine high protonic conductivity, low permeability to fuel, good mechanical properties and thermal stability in hot oxidative atmospheres is nowadays a flourishing field of research.

On the other hand, concerns regarding the environmental impact of synthetic materials and the depletion of the raw

* Corresponding author. Tel.: +34963879328; fax: +34963877924.
E-mail address: vicommo@ter.upv.es (V. Compañ).

http://dx.doi.org/10.1016/j.jpowsour.2014.04.093
0378-7753/© 2014 Elsevier B.V. All rights reserved.

materials, mainly fossil fuels, used for their preparation are becoming nowadays a serious issue, in particular for areas in which a growing industrial demand is expected. This highlights the relevance of developing environmentally friendly materials, like biomaterials derived from natural sources such as polysaccharides, proteins and/or lipids. Among these, the use of polysaccharides is of particular interest in this field, and the use of chitosan, pectin, alginate and carrageenan, between others, for the preparation of membranes, is attracting much attention.

The use of bio-polymer membranes in the field of fuel cells depends upon several features such as cost, availability, performance characteristics, mechanical properties (strength and flexibility), the requirements of barrier properties (permeability to methanol and proton conductivity), and water resistance. These characteristics are greatly influenced by parameters such as the material used for the structural matrix or the type and concentration of additives (plasticizers, crosslinking agents, sulfonating agents and so on) [7–9].

Recently, proton conducting composite membranes were produced using chitosan and methanediphosphonic acid (Chitosan/MP) and obtaining polymer composites of Chitosan and poly(vinyl phosphonic acid) (Chitosan–PVPA) [10],. These materials have a methanol permeability lower than Nafion® 115, but the proton conductivity measured was approximately 3×10^{-5} S cm^{-1} at 120 °C in the anhydrous state. Another membrane prepared from Chitosan with an anionic polyelectrolyte, acrylic acid-2-acrylamido-2-methylpropane sulfonic acid copolymer P(AA-AMPS) exhibited a methanol permeability of 2.41×10^{-7} cm^2 s^{-1} much lower than that of Nafion® 117 membrane, whereas its proton conductivity was moderately high: 3.6×10^{-2} S cm^{-1} [11].

Alginates are natural substances extracted from brown algae and composed of 1,4-D-manuronic acid (M) and L-guluronic acid (G). In the polymeric chain, the monomers are arranged alternately in MM GG and MG blocks. The chemical composition and sequence of the M and G blocks depend on the biological source, growth and seasonal conditions [12]. Due to their particular colloidal properties, the alginates are used as bio-polymer films. The carrageenan is a bio-polymer extracted from algae and is used extensively in the food industry for the formation of gels and emulsions to stabilize fat in milk, ice cream and milk shakes. There are three main carrageenans that differ only in the number of sulfonic groups. The κ-carrageenan is mostly ionic and adopts a helical conformation independently of the ionic strength and temperature. The Kappa and Iota carrageenans form gels, but the λ-lambda carrageenan does not form gels and is used as such as a thickener [13,14]. κ-carrageenan cannot form films of good quality, but having a considerable amount of sulfonic groups in their structure makes this material attractive for the development of PEM. The main drawbacks of these polymeric membranes are their poor mechanical properties and high solubility in aqueous media. In order to improve mechanical properties and reduce the solubility of these polymers in water it is necessary to crosslink the polymer matrix. Different functional groups of these polysaccharides, like the –OH or –COOH groups, allow the reaction with Glutaraldehyde (GTA), ions (Ca^{2+}, K^+) or diimine, among others [15], generating a crosslinked film. GTA is the most commonly used agent due to its high reactivity in aqueous solutions. Carrageenan and alginate membranes have been used in many types of applications such as separation of water–alcohol mixtures, enzyme immobilization and controlled drug release [16–21], but their application as polymer polyelectrolyte membranes never has been studied.

The objective of this work was to prepare membranes from different compositions of Alginate and κ-carrageenan for DMFC at low temperatures. Those films were crosslinked and sulfonated and then characterized by several techniques including ionic exchange capacity (IEC), water uptake and mechanical and thermal properties. Functional properties such as methanol permeability, proton conductivity and Direct Methanol Fuel Cell tests at 50, 70 and 90 °C with a methanol feed concentration of 2 M were also determined.

2. Experimental

2.1. Preparation of membranes

The membranes were synthesized from pure solutions of alginate, carrageenan and mixtures thereof, Fig. 1a. Those neat two solutions were prepared by dissolving the polymers at 2% (*w*/*v*) in water at 40 °C. With appropriated amounts of each solution, mixtures of different ratios were prepared in order to obtain films named Alg/Car 100/0, 95/05, 90/10 and 80/20. Beyond this concentration ratio (i.e. more than 20% of carrageenan) films were partially soluble in water. Glycerol was added as plasticizer at 0.5%. Then, membranes were cast by placing the solutions in petri dishes of diameter 14.5 cm. Membranes were obtained after drying at 60 °C for 24 h. The films obtained were crosslinked by soaking in a solution of 50 mL of acetone (Biopack) containing 5% (*w*/*v*) glutaraldehyde 25% grade II (Sigma) and 1% *w*/*v* HCl (Alkemir) for 22 h. If more glutaraldehyde concentration is added so brittle films were obtained. Finally, the films were washed several times with ethanol and distilled water.

2.2. Chemical functionalization

In order to increase the ionic groups in the films, the obtained membranes were immersed in a 0.04 M 4-formyl-1,3-benzenedisulfonic acid disodium salt (Aldrich) aqueous solution containing 0.1 M HCl as a catalyst for the sulfonation reaction showed in Fig. 1b.

The reaction was carried out at 50 °C for 2 h. Then, the possible residual sodium ions present on the surface of the functionalized membrane were exchanged by H^+ immersing the films into a 0.3 M HCl solution in isopropanol/water (70/30 *v*/*v*) for 24 h. Then they were repeatedly washed with a solution of isopropanol/water (70/30 *v*/*v*). Finally, the membranes were dried at 50 °C, overnight.

3. Membranes characterization

3.1. Ionic exchange capacity

Each prepared membrane was kept in contact with a 0.1 M HCl aqueous solution for 12 h. The acidic membranes were then washed several times with distilled water and then immersed into a 1 M NaCl aqueous solution. After that, they were titrated with a 0.01 M NaOH aqueous solution to determine the concentration of exchanged protons. IEC was expressed as meq H^+ g^{-1} of dry membrane and the results are shown in Table 1.

3.2. Water uptake

Water uptake of the Alg/Car membranes was measured at 25 °C by first weighting (W_d) the H^+-form samples thoroughly dried in a vacuum chamber. Then, they were immersed in distilled deionized water overnight. After that, the membranes were removed from water, gently dried with a paper cloth to remove excess surface water, and then weighed again (W_w). This operation was repeated five times. Water uptake was obtained by means of the expression (1) and the values referred to the wet membrane are given in Table 1.

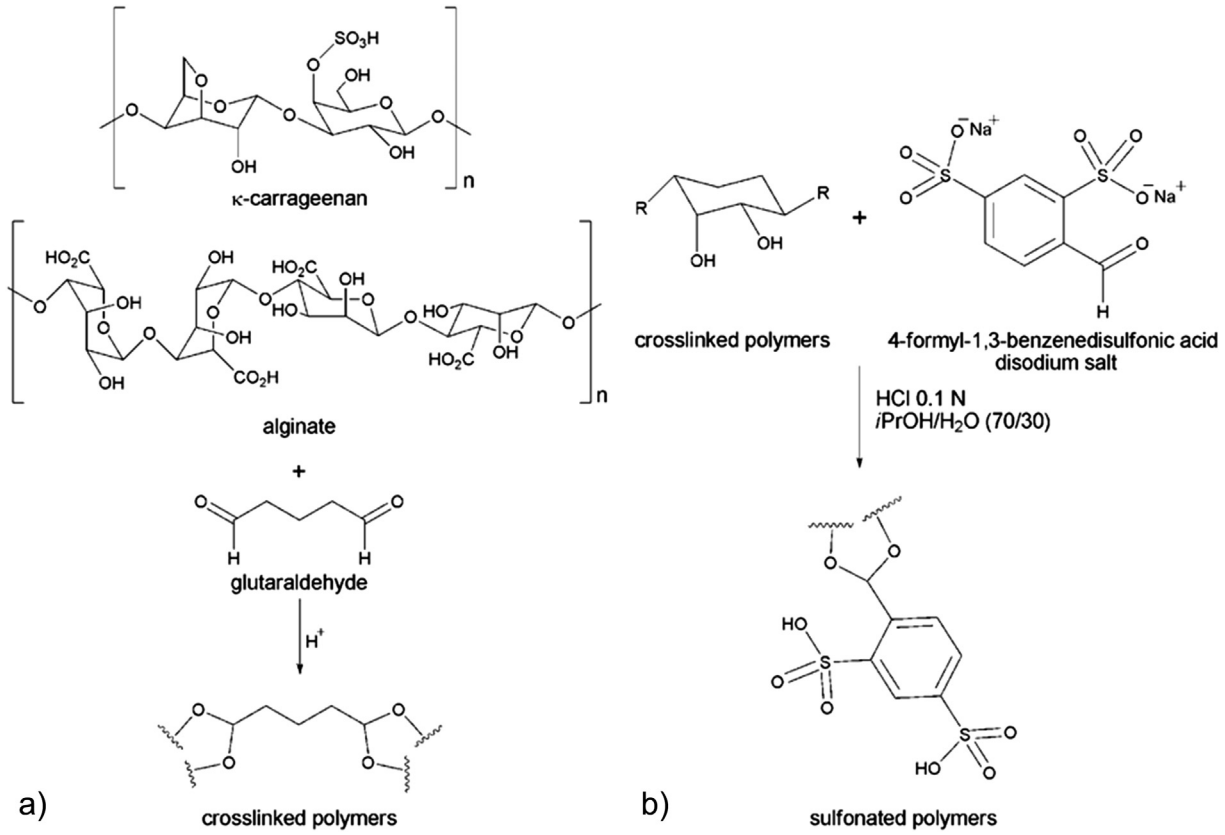

Fig. 1. Schematic representation reaction of: a) membrane chemical functionalization and b) membrane sulfonation.

Table 1
Water uptake and ionic exchange capacity (IEC).

Membrane	Water uptake (%)	IEC (meq g^{-1})
Alg/Car 100/0	146.1 ± 0.1	0.59 ± 0.01
Alg/Car 95/05	149.2 ± 0.1	0.65 ± 0.01
Alg/Car 90/10	165.2 ± 0.1	0.83 ± 0.01
Alg/Car 80/20	234.1 ± 0.1	1.15 ± 0.01

$$\text{Water uptake} = \left(\frac{W_w - W_d}{W_d}\right)\cdot 100 \quad (1)$$

3.3. Infrared spectroscopy

Fourier transform infrared spectroscopy (FTIR) spectra were measured at 25 °C using Nicolet Protégé model 460 spectrophotometer, provided with CsI beam splitter between 4000 and 225 cm^{-1}. A total of 128 interferograms, at a resolution of 4 cm^{-1}, was acquired. Dry samples were measured after chemical functionalization, stabilized for 12 h into 0.1 M HCl aqueous solution and dried at 40 °C.

3.4. Elemental analysis

Elemental analysis was performed with a scanning electron microscope (SEM) LEO 1450VP using an EDS Genesis 2000 (EDAX) energy dispersion X-ray analysis. Three samples of each membrane with surface of areas 5 × 5 μm^2 were analyzed.

3.5. Mechanical properties

Static tensile strength tests were carried out at room temperature using a Microtest Tensile stage controller DEBEN (Gatan). A crosshead rate of 0.4 mm min^{-1} collecting data each 500 mS was used in each measurement. The separation between the clamps was fixed at 10 mm and the maximum force was set at 150 N with an initial static force of 0.1 N. The samples were cut in pieces of 15 × 10 mm and measurements of thickness and width were conducted by means of a length calibrator. All the measurements have been done to ambient temperature. The membrane thickness was calculated from the average value after measured five measurements on different parts of the sample and its error represents the standard deviation obtained.

3.6. Differential scanning calorimetry (DSC)

The DSC curves were obtained at 10 K min^{-1} under a nitrogen atmosphere (Mettler Toledo DSC 831). Two scans were performed with each sample being the first from −50 °C to 80 °C in order to remove the thermal history of the samples, and the second from −50 °C to 500 °C.

3.7. Membrane conductivity

The resistances of the membranes were measured by impedance spectroscopy at 30, 50, 75 and 90 °C, in the frequency range $10^{-1} < f < 10^{7}$ Hz with 0.1 V amplitude, using a Novocontrol broadband dielectric Spectrometer (Hundsangen, Germany) integrated by a SR 830 lock-in amplifier with an Alpha dielectric interface. The membrane sample, equilibrated with water, was

placed between two gold electrodes coupled to the spectrometer integrated by a SR 830 lock-in amplifier with an Alpha dielectric interface. The temperature was controlled by a nitrogen jet (QUATRO from Novocontrol) with a temperature error of ≈0.1 K during every single sweep in frequency. The measurements were performed at the temperatures of interest under 100% RH [22]. To obtain the conductivities of the membranes, four runs for each temperature were made. Seeing that the reproducibility of the results was satisfied, the conductivity was obtained by taking the average of all measurements and their error as the mean-square deviation.

3.8. Methanol permeability by densimetry

In order to determine the methanol permeability coefficient through the composite membranes, an experimental set-up as shown in Fig. 2 was used. The apparent methanol permeability of the membranes was measured at 50 °C by density measurements. The variation of methanol concentration with time in the receiver reservoir (C_B) was determined by means of a densimeter (DMA 4500M). The membrane sample (≈1 mL) was introduced into a U-shaped borosilicate glass tube that was being excited to vibrate at its characteristic frequency, which changed according to the material density. Through a precise determination of the characteristic frequency and a mathematical conversion, the mass density (g cm^{-3}) of the sample can be given. A calibration curve of density vs. methanol concentration was obtained before the permeation measurements. During those experiments, a small sample of solution from the receiver compartment was taken at certain time intervals and the density recorded. In order to avoid changes in the volume of liquid in the receiver reservoir (V_B), the samples were recovered from the densimeter after each measurement. Representing C_B vs. time, the flux (J) and apparent permeability (P) of the methanol across the membranes can be determined.

3.9. Methanol fuel cell performance of composite membrane Alg/Car 80/20

MEAs prepared with Alg/Car 80/20 membranes of 150 μm thickness were tested in the single cell hardware described previously [23].

The anode and cathode were acquired from BalticFuelCells GmbH (Schwerin, Germany). The anode is composed of a carbon paper gas diffusion layer (GDL) from Freudenberg&Co (Weinheim, Germany), model H2315 T105A, covered by an alloy of Pt–Ru black 50:50 (Alfa Aesar) with a catalyst loading of 5.0 mg cm^{-2} together with a 20 wt% of dry Nafion® ionomer. Similarly, the cathode was composed of a GDL from Freudenberg, model H2315 I3C4, with a catalyst loading of 5.0 mg cm^{-2} of Pt, containing platinum nanoparticles (≈5 nm size) supported by advanced carbon (HiSPEC 13100, Alfa Aesar) with a Pt/C ratio of 70% (weight) and a 20 wt% of dry Nafion® ionomer.

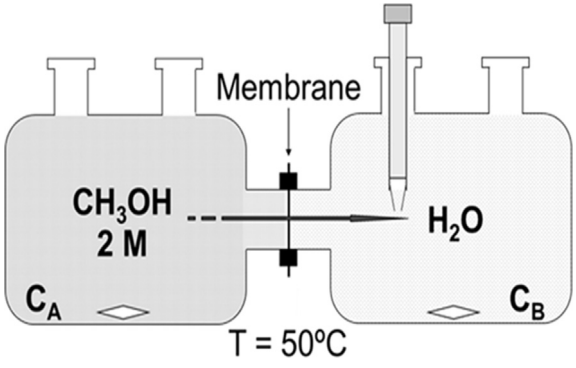

Fig. 2. Schematic representation of the experimental set-up used for determination of the methanol permeability across the membranes.

The MEAs, previously equilibrated with water, were placed into a square 5 cm^2 active area fuel cell hardware (quickCONNECT, BalticFuelCells GmbH) containing graphite serpentine flow fields and equipped with a pressure-controlled clamping force system. This latter characteristic enables to exert a constant contact resistance between membrane and electrodes.

The anode side of the cell was flooded with deionized water to prevent dryness of the membrane, and thus, fully hydrated conditions were assured in the measurements. No gases were flowing across anode and cathode during the experiments.

A 2 M methanol solution in water pumped at a flow rate of 5 mL min^{-1} was used to feed the anode. The cathode was fed with oxygen from the surrounding air at a flow rate of 150 mL min^{-1} and atmospheric pressure.

I–V curves (current density vs. potential) were obtained at 50, 70 and 90 °C from OCV (open circuit voltage) conditions up to 0.2 V by manual stepwise increment of the current density and waiting for 2 min in each measurement in order to assure the reading of a voltage near a steady-state value. Power density values were thus calculated and represented. Before I–V measurements, the MEAs were activated for 5–6 h by alternating different current demands until a stable operation was achieved. This is helpful to open new pores and channels into the catalytic layers so more fuel and oxygen can reach the catalyst particles and enhance performance of the electrodes.

4. Results and discussion

In general the conductivity of acidic membranes involves dissociation of proton from $-SO_3H$ groups and their transport across water and $-SO_3^-$ ionic fixed groups. Then, the conductivity depends on the water uptake and the Ionic Exchange Capacity (IEC) of the membranes. Values of the water uptake and the IEC obtained for all the studied membranes are given in Table 1. The results obtained for the water uptake show that this parameter is very dependent on the amount of carrageenan when the composition of carrageenan is higher than 15%. The pure Alg/Car 100/00 membrane had the lowest water uptake. When the content of carrageenan in the composite membranes increases up to 15% produces an increase of water uptake about 50% and also the IEC increases by almost a 95% presumably as a consequence of the critical balance between the two phases. Thus, water is both attached to the sulfonic acid groups of carrageenan and incorporated into the alginate chemical structure.

From the FTIR spectrum of Alg represented in Fig. 3, we can see a broad peak at 3450 cm^{-1} that is due to the stretching vibrations of O–H, and a small peak at 2930 cm^{-1} is attributed to the C–H stretching vibrations of methine groups. The bands at 1100 and 1040 cm^{-1} are assigned to C–O–C stretching vibrations of the saccharide structure [24,25]. It is further noted that two strong peaks at 1635 and 1429 cm^{-1} are assigned to asymmetric and symmetric stretching vibrations of carboxyl groups present in Alg. Common bands with κ-carrageenan are 3450, 2930 and 1040 cm^{-1}. The κ-carrageenan spectrum presents a characteristic band at 1225 cm^{-1} due to the S=O of sulfate stretch. However, all spectrum in Fig. 3 contains not only the characteristic Alg and Carr bands, but also features additional peaks. The small peak of 2850 cm^{-1} is usually assigned to aliphatic C–H stretching vibrations and the peaks of 1745 and 1250 cm^{-1} are attributed to the C=O and C–O component of an ester bond respectively [26,27]. The appearance of

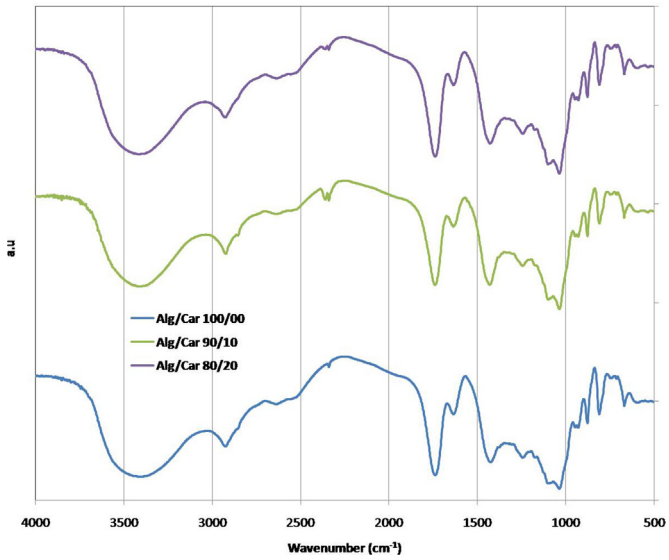

Fig. 3. FTIR spectrums of Alg/Car membranes.

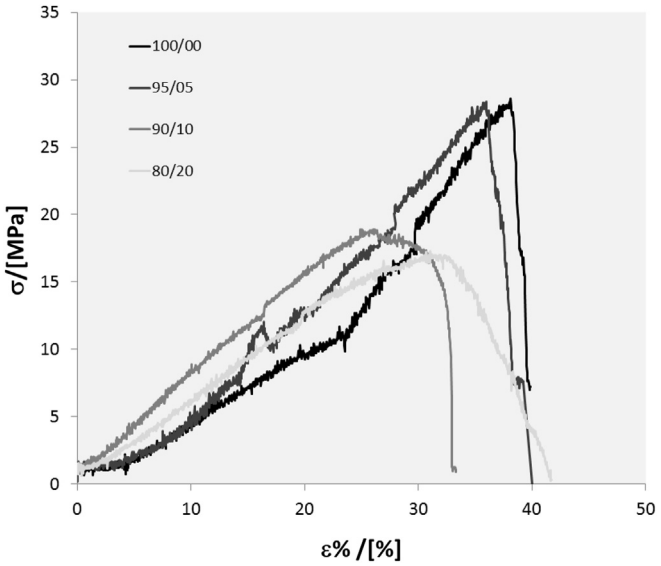

Fig. 4. Stress–strain curves for Alg/Car membranes: Alg/Car 100/00 (black color), Alg/Car 95/05 (red color), Alg/Car 90/10 (green color), Alg/Car 80/20 (blue color). (For interpretation of the references to colour in this figure legend, the reader is referred to the web version of this article.)

the peaks suggests that isopropanol groups were esterificated onto alginate during sulfonation. Alginate esterification causes an increase of hydrophobic character in all films conducting to a moderate augment of SI despite its higher IEC.

As we can see in Fig. 3 the Ester signals overlap $-SO_3$ group signals and it was therefore necessary to determine $-SO_3$ groups by elemental analysis. Table 2 shows the average composition of C, O and S in each membrane analyzed. The amount of C, O and S elements was identified demonstrating that sulfonation reaction was carried out, especially in Alg/Car 100/0. In all membranes, S content was according to IECs results.

Static mechanical testing of the samples was also performed and the results of stress vs. strain are presented in Fig. 4 for Alg/Car membranes. A close inspection of this figure shows lower values of ultimate tensile (σ_{ult}) and yield strength (ε_y) as thickness increases. Strain values follow a similar trend. The values of strain found for the Alg/Car membranes are remarkable, which can explain the well-known ductile behavior associated to this kind of bio-polymers in comparison with other membranes used as polyelectrolyte membranes in fuel cells applications. For example, for a Nafion® membrane of 60 μm thickness prepared by casting, we have obtained values for the ultimate tensile strength of 31 MPa, similar to those of Alg (28 MPa) and Alg/Car 95/05 (28 MPa) membranes, respectively [28,29].

In Table 3 we show the mechanical parameters obtained from Fig. 4 for Alg/Car membranes. In all cases, the mixed membranes of Alg/Car show lower values of ε_y, σ_{ult} and Young's modulus (E) than sulfonated alginate membrane. This effect reveals that the loss of mechanical stability of films was achieved by the incorporation of carrageenan into the alginate matrix. When the content of carrageenan increases up to 5% produces an increase of the water uptake of the membranes producing a decreasing of Young's modulus of about 50% and the ultimate tensile strength, σ_{ult} decreases about 42%.

DSC thermograms of sulfonated Alg/Car membranes with compositions 100/00, 95/05, 90/10 and 80/20 are shown in Fig. 5. The left inset shows curves indicating the glass transition temperature (T_g) of the membranes. The T_g values of the membranes are 72, 75, 76 and 72 °C for membranes with Alg/Car compositions of 100/00, 95/05, 90/10 and 80/20, respectively. The results indicate that low concentrations of carrageenan have a very weak thermoprotective effect, which slightly delays the polymer glass transition. This effect is not evident in compositions of 20% of carrageenan. In the right inset, the temperature scale is expanded between 100 and 250 °C. It can be seen that the Alg/Car 100/00 membrane has a melting temperature (T_m) of 170 °C whereas membranes Alg/Car 95/05, Alg/Car 90/10 and Alg/Car 80/20 have T_m values at 175, 188 and 170 °C respectively, following the tendency found in T_g, where the thermoprotective effect is revealed for low carrageenan contents. This effect can be the result of a major cohesion between the polysaccharide chains. When carrageenan content was higher than 20 wt% we have observed that the films starting to loss chemical stability in acid media to be partially soluble in water.

In order to determine the methanol permeability coefficient through the composite membranes, an experimental set-up as

Table 2
Elemental analysis of membranes from EDS analysis.

Membrane	Element	wt %
ALG/Car 100/00	C	53.6
	O	46.0
	S	0.4
ALG/Car 95/05	C	52.0
	O	47.1
	S	0.9
ALG/Car 90/10	C	50.2
	O	48.0
	S	1.8
ALG/Car 80/20	C	48.0
	O	49.0
	S	3.0

Table 3
Mechanical parameters, membrane thickness, strain at yield point (ε_y), ultimate tensile strength (σ_{ult}) and Young's modulus (E) of sulfonated Alg–Car membranes.

Sample	L (μm)	ε_y (%)	σ_{ult} (MPa)	E (MPa)
100/00	148 ± 2	37.39 ± 0.7	28.05 ± 0.3	1.21 ± 0.03
95/05	138 ± 2	35.19 ± 0.5	28.03 ± 0.5	0.79 ± 0.02
90/10	208 ± 2	25.18 ± 0.7	18.80 ± 0.4	0.73 ± 0.02
80/20	221 ± 2	30.26 ± 0.5	16.86 ± 0.2	0.63 ± 0.01

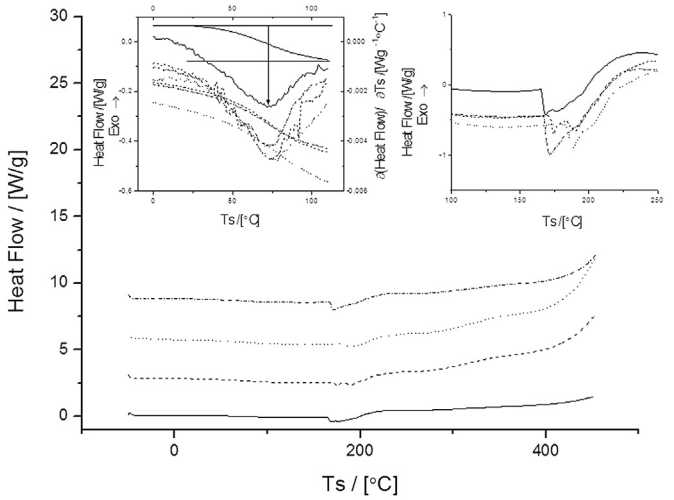

Fig. 5. DSC thermograms of Alg/Car membranes. In the left inset T_g area. In the right inset, T_m area. In all cases, solid line Alg/Car 100/00, dash line Alg/Car 95/05, dot line Alg/Car 90/10, and dash dot line Alg/Car 80/20.

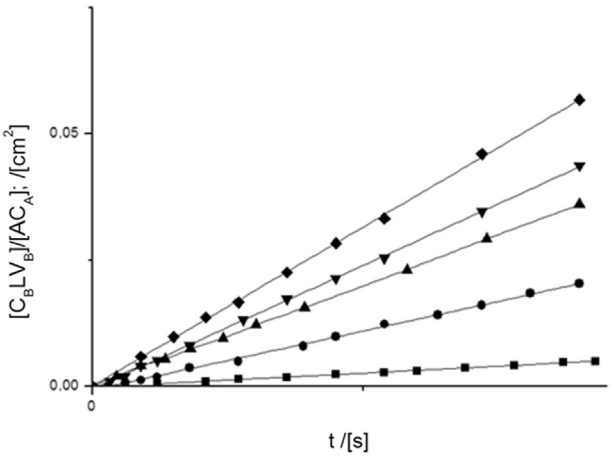

Fig. 6. Normalized methanol concentration vs. time at the permeability experiments for sulfonated alginate/carrageenan membranes. Alg/Car 100/00 (■), Alg/Car 95/05 (●), Alg/Car 90/10 (▲), Alg/Car 80/20 (▼), Alg/Car 75/25 (◆).

shown in Fig. 2 was used. Chamber A was filled with a 2 M aqueous solution of methanol, while chamber B was filled with bi-distilled water. Both chambers were kept under stirring and thermostatized at 50 °C. A sample of 1 mL from chamber B was taken every certain time and then introduced into the densimeter (DMA 4500M) above described. Before permeability measurements seven samples containing different methanol concentrations in water were prepared and their densities measured at 25 °C to obtain the calibration curve. Using this calibration curve and under the same conditions and experimental set-up as mentioned above, the change in the methanol concentration as a function of time was obtained following the same procedure described before [28]

$$C_B = \frac{P \cdot A}{L \cdot V_B} C_A \cdot t \tag{2}$$

where P is the apparent permeability coefficient ($cm^2\ s^{-1}$), C_B is the methanol concentration in chamber B, C_A is the methanol concentration in chamber A (in our study this value is 2 M), L represents the membrane thickness, A is the area of exposed membrane (2.27 cm^2), V_B is the volume of water filling the chamber B (150 cm^3) and t is the time for each measurement (s).

The results for each one of the membranes studied is shown in Fig. 6. In this plot we represent the normalized methanol concentration ($C_B \cdot L \cdot V_B/(A \cdot C_A)$) vs. time. The apparent permeability coefficients (P) were determined from the slope of eq. (2) and the pertinent results are given in Table 4.

A close inspection of Table 4 shows that the apparent permeability of methanol for sulfonated Alg/Car membranes increases with the carrageenan content, presumably due to the increasing of water content. These values are quite similar to values found for pristine Nafion® ($P \approx 2.19 \times 10^{-6}$ $cm^2\ s^{-1}$) but higher than for a Nafion/PVA membrane ($P \approx 5.98 \times 10^{-7}$ $cm^2\ s^{-1}$) [30].

The complex dielectric function $\varepsilon^*(\omega,T)$ is equivalent to the complex conductivity function $\sigma^*(\omega,T)$ expressed as $\sigma^* = j\omega\varepsilon_0\varepsilon^*$ where $\varepsilon^*(\omega) = \varepsilon'(\omega) - j\varepsilon''(\omega)$ and $\sigma^*(\omega) = \sigma'(\omega) + j\sigma''(\omega)$, where ε_0 is the vacuum permittivity and j is the imaginary unity ($j = (-1)^{1/2}$). Thus, both formalisms should permit us to explain the behavior of the mechanism of transport of the protons through the membranes. Fig. 7 shows the log–log plots of the real ε' and complex ε'' (dielectric loss) part of the complex dielectric permittivity ε^* and the real σ' and imaginary σ'' parts of the conductivity as a function of the frequency for the sulfonated Alg/Car 90/10 membrane at temperatures of 30, 50, 75 and 90 °C, respectively. For the dielectric loss ε'' three different regions can be observed at high, medium and low frequencies, respectively. Similar conclusions can be seen from the log–log plot of the imaginary part of the conductivity ($\sigma''(\omega)$). For high frequencies, the dependence is almost linear with the slope being very close to unity showing the contribution to the electrical conduction [31,32] of proton transport through the membrane. For intermediate frequencies, in the range ($10^4 \leq f \leq 5 \times 10^5$) we observe a shoulder or a peak depending of the temperature. This can be explained as a Debye relaxation due to the macroscopic polarization of the ionic charges in the alternating electric field [32–35], characterized by a time relaxation practically independent of the temperature, decreasing with the carrageenan content from 0.1 μs for pristine alginate to 40 μs for Alg/Car 80/20 sulfonated membranes. The Debye shoulders shift very slowly to lower frequencies as the temperature decreases. At low frequencies, the dependence is again linear, but with a slope lower than unity; this is an indication of a dependence of the type MWS [36–38]; $\varepsilon'' = \sigma'/\varepsilon_0\omega^n$, with ε_0 is the vacuum dielectric permittivity, ω is the angular frequency and $n \leq 1$. It is observed that $\sigma'(\omega)$ decreases from σ_{dc}, and it is considered a parameter directly related to some conductivity due to the electrode polarization resulting from blocking electrodes of charge carriers. The σ_{dc} conductivity value corresponding to the plateau observed at high frequencies is observed for a characteristic frequency ($\omega_c = 2\pi f_c$) at which dispersion sets in and turns into a power law at higher frequencies. On the other hand, if we observe the log–log plot of the real part of the dielectric permittivity at f_c turns from the high frequency limit to the static value ε_R.

In Fig. 8 we can see the values obtained for the static permittivity ε_R of the membranes. From this plot we can observed that the static permittivity increases linearly when the temperature increases for all membranes containing different concentrations of carrageenan. Also from the inset we observe that the static

Table 4
Apparent permeabilities of methanol at 50 °C for several of Alg/Car membranes.

Sample	L (μm)	P ($cm^2\ s^{-1}$) × 10^6
Alg/Car 100/00	250 ± 2	0.55 ± 0.02
Alg/Car 95/05	158 ± 2	2.34 ± 0.03
Alg/Car 90/10	174 ± 2	4.00 ± 0.03
Alg/Car 80/20	261 ± 2	4.89 ± 0.03

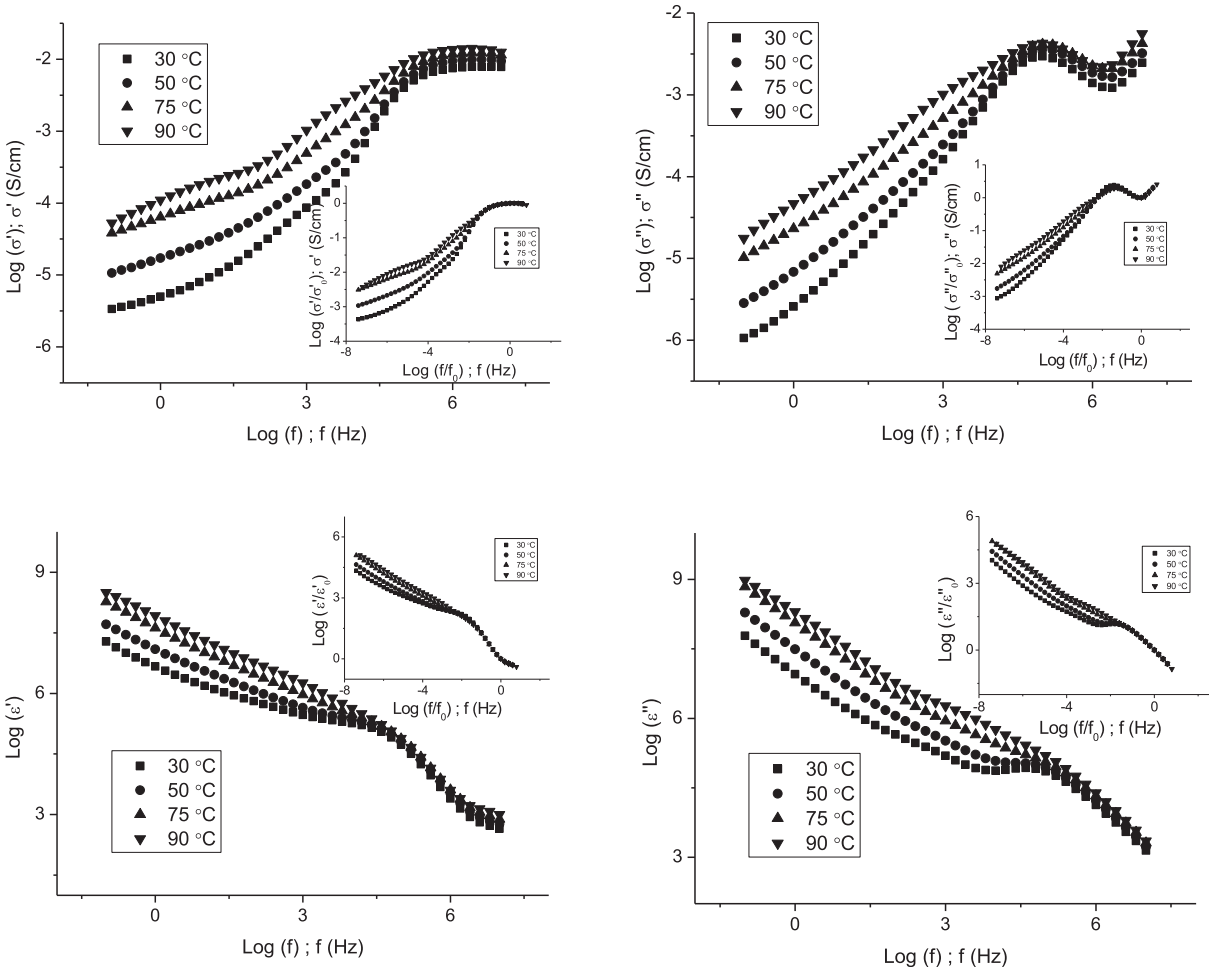

Fig. 7. Log–Log plots of the real ε' and complex ε'' part of the complex dielectric permittivity ε^* and the real σ' and imaginary σ'' parts of the conductivity as a function of the frequency for sulfonated membrane Alg/Car 90/10 at temperatures of 30, 50, 75 and 90 °C.

permittivity increases moderately with the Carrageenan content until the amount of Alginate is below 20%. A percolation phenomenon is observed, presumably because of the critical balance of the Alginate and Carrageenan phases that can be present, as is also observed with the changes of water uptake and IEC shown in Table 1.

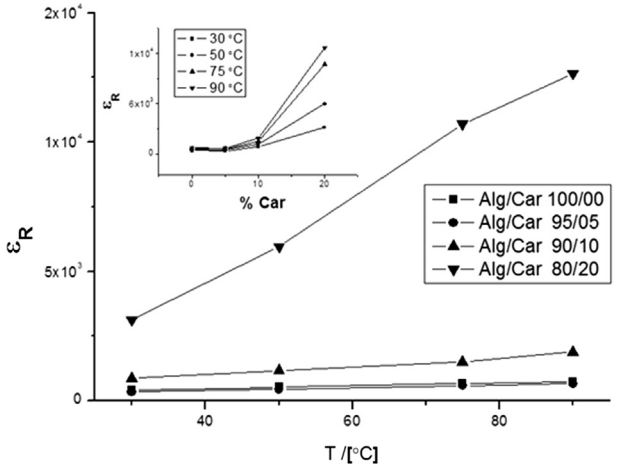

Fig. 8. Static permittivity, ε_R, vs. temperature for all the samples. The inset shows the variation of the static permittivity vs. the % Alg/Car for all temperatures.

When scaling with respect to σ_{dc} and ω_c, it is remarkable that the spectra are coincident in normalized log–log plots, as is shown in the inset. This indicates that the mechanism of proton transport through the membranes follows an identical underlying mechanism for all the samples studied in this work. On the log–log plots of ε', ε'', σ' and σ'' vs. frequency, it is observed that the amount of Carrageenan does not significantly modify the strength and the conductivity of the samples.

Traditionally the equivalent circuit describing the response of the assembly electrodes-membrane to an alternate electric field $E = \mathrm{Im}\,(E_0 \cdot \exp \cdot j\omega t)$, where ω is the angular frequency, consists of a resistance R_0 that accounts for the proton resistance in the membrane in series with a circuit, made up of a resistance R_p (representing a polarization resistance) in parallel with a constant phase element (CPE) of admittance $Y^* = Y_0(j\omega\tau)^n$ $(0 < n \leq 1)$ [39]. This CPE accounts the interfacial phenomena in the membrane–electrode interface. The impedance of the circuit is given by

$$Z^* = R_0 + \frac{R_p}{1 + R_p Y_0 (j\omega\tau)^n} \tag{3}$$

where $\tau = RC$ is the relaxation time. The plot Z'' vs. Z', called Nyquist diagram is a semicircle that intersects the abscissa axis at $Z' = R_0$ and $Z' = R_0 + R_p$ in the extreme values of frequency $\omega \to \infty$ and

$\omega \rightarrow 0$, respectively. An alternative plot that was used here is the Bode diagram. In this case the frequency dependence of the complex impedance, $|Z^*|$, decreases from R_p at $\omega \rightarrow 0$ to R_0 at $\omega \rightarrow \infty$. Moreover, the out of phase angle $\phi = \tan^{-1}(Z''/Z')$ increases with increasing frequency reaching a maximum ($\phi = 0$) at $\omega \rightarrow \infty$. The resistance R_0 was taken as the value of $|Z^*|$ at the frequency at which $\phi = 0$.

Fig. 9 shows the Bode diagrams in terms of conductivity for the Alg–Car 95/05 membrane at 30, 50, 75, and 90 °C. An inspection of the curves shows that the values of conductivity and ϕ (phase angle) reach a plateau and a maximum in the high frequency region, respectively. The value of the conductivity obtained represents the proton conductivity of the membrane. Alternative Nyquist diagrams permit us to determine the real part of the impedance, and knowing the sample thickness (L), and the area of the membrane in contact with the electrodes (S), the real part of the conductivity is obtained ($\sigma' = L/(Z' \cdot S)$). In the inset of Fig. 9 we plot the Nyquist diagram for the same temperatures represented in the Bode diagram of conductivities. In this figure the real and imaginary components of the complex impedance are plotted for all the range of frequencies. We can observe for all temperatures semicircles intersecting the abscissa axis in the high frequency region at $Z' = R_0$ (i.e. the membrane resistance). Departure from semicircles is observed as a result of polarization processes and other phenomena taking place in the membrane–electrode interface. The solid line that appears in the inset is the fit Z'' vs. Z' (obtained following the expression 3) to the experimental complex data in a relatively wide range of the high frequency region. The parameters Y_0, n and R_p of the fit are given in Table 5. In this table all the conductivities for the membranes at several temperatures are also collected.

As could be expected, the conductivity of the membranes increases with temperature up to 1.8–2.0 times. When we compare the different membranes, it can be observed how the conductivity increases with the amount of the carrageenan component present. Up to a 3.2 fold increase can be found in this regard. For example, the conductivities at 90 °C of the membranes Alg/Car 80/20 and Alg/Car 100/00 are 3.2×10^{-2} and 9.8×10^{-3} S cm^{-1}, respectively.

Proton transport in acidic membranes is a complex process involving dissociation of the proton from the fixed sulfonic acidic group, its transference to the first hydration shell water molecules, separation of the hydrate proton from the conjugate base (anion of the acid group) and diffusion of the proton presumably stabilized as Eigen-like cation in the confined water in the membrane matrix [40,41]. Moreover the large scale connection of the water domains within the hydrated membrane and the flexibility of the skeletal bond of the polyelectrolyte chains favor proton transport in the acidic membranes. It can be expected that sulfonated molecules trapped in alginate domains might connect hydrophilic domains thus favoring proton transport. For composite Alg/Car membranes the values of the water uptake and IEC increase when the carrageenan content increase due to increasing of hydrophilic domains produced by the alginate for all the temperatures of interest.

Fig. 10 show the Arrhenius plots for the Alg/Car membranes. In Table 6 we can see the values of the activation energy of the membranes studied in this work. From this table we can conclude

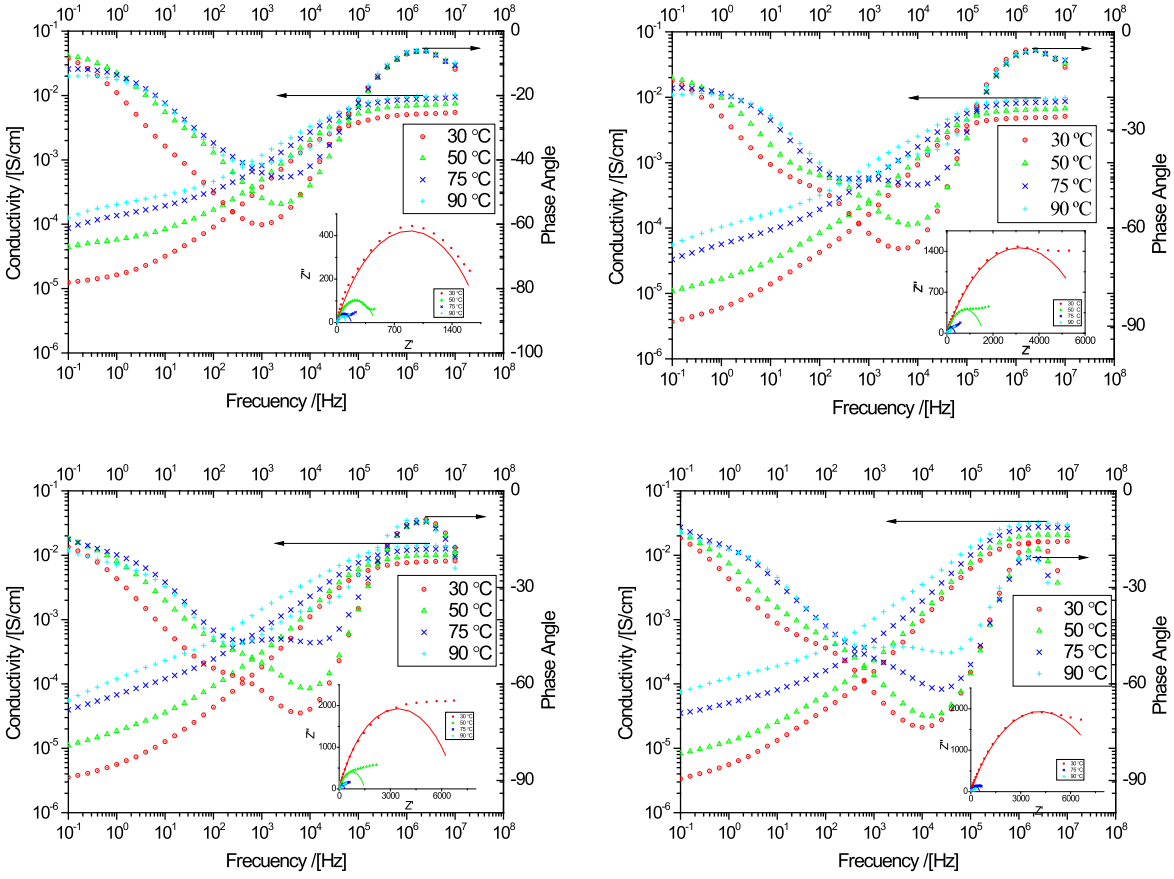

Fig. 9. Bode diagrams for the Alg/Car membranes at several temperatures: 30, 50, 70 and 90 °C. Alg/Car 100/00 (top left), Alg/Car 95/05 (top right), Alg/Car 90/10 (bottom left), Alg/Car 80/20 (bottom right). The inset show the Nyquist plots for the same membranes. The lines in the inset figures joining the experimental results for both Z'' vs. Z' obtained following the eqs. (4) and (5).

Table 5
Values of the protonic resistance and conductivity of the membranes obtained from Nyquist diagrams. The values of Y_0, n and τ are the parameters of adjust to the experimental date.

Alg/Carr 100/00						
T (°C)	R_0 (Ω)	R_p (Ω)	Y_0	$\tau_0 \times 10^4$ (s)	n	$\sigma \times 10^3$ (S cm^{-1})
30	2.72	1770.6	4.1	48.5	0.57	5.2
50	1.98	474.4	6.6	5.6	0.51	7.1
75	1.58	179.5	9.1	1.5	0.54	8.9
90	1.44	112.4	6.4	2.3	0.61	9.8
Alg/Carr 95/05						
T (°C)	R_0 (Ω)	R_p (Ω)	Y_0	$\tau_0 \times 10^3$ (s)	n	$\sigma \times 10^3$ (S cm^{-1})
30	2.9	6301.8	4.2	12.1	0.55	4.9
50	2.2	1593.0	2.7	8.6	0.60	5.5
75	1.7	360.8	1.1	8.0	0.62	8.3
90	1.5	195.1	1.0	8.0	0.61	9.4
Alg/Carr 90/10						
T (°C)	R_0 (Ω)	R_p (Ω)	Y_0	$\tau_0 \times 10^3$ (s)	n	$\sigma \times 10^3$ (S cm^{-1})
30	2.2	6873.8	4.4	10.4	0.65	0.8
50	1.7	1490.2	2.7	6.1	0.64	1.0
75	1.4	325.8	1.2	5.6	0.65	1.3
90	1.2	172.3	1.0	7.1	0.66	1.4
Alg/Carr 80/20						
T (°C)	R_0 (Ω)	R_p (Ω)	Y_0	$\tau_0 \times 10^2$ (s)	n	$\sigma \times 10^2$ (S cm^{-1})
30	1.0	8351.0	4.8	1.3	0.55	1.6
50	0.8	–	–	–	–	2.1
75	0.6	530.9	0.7	2.4	0.60	2.7
90	0.5	197.3	0.6	1.9	0.66	3.2

Table 6
Diffusion coefficient (D_+) obtained from eq. (4) at 30, 50, 75 and 90 °C. The activation energy and the ratio proton conductivity of the membrane over methanol permeability, β, for a concentration of 2 M in donor chamber is also reported for each sample.

Sample Alg/car	$D_+ \times 10^6$ (cm^2 s^{-1})				E_{act} (Kcal mol^{-1})	$\beta = \sigma/P$ (S s cm^{-3})
	$T = 30$ °C	$T = 50$ °C	$T = 75$ °C	$T = 90$ °C		$T = 50$ °C
100/00	2.4	3.5	4.7	5.4	2.3	12,960
95/05	2.3	3.4	4.7	5.6	2.3	2730
90/10	2.6	3.5	4.7	5.5	2.3	2500
80/20	3.8	4.9	7.2	8.9	2.0	4200

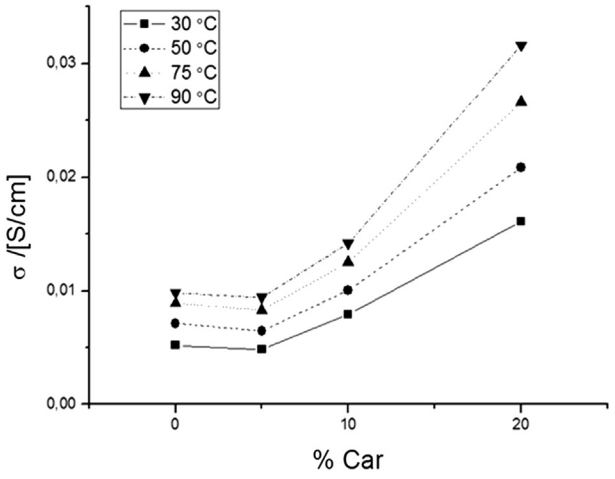

Fig. 11. Membranes conductivity vs. carrageenan content (%) at several temperatures.

that the amount of carrageenan in membranes does not produce significant changes in the energies of activation. The values of the activation energy follow the tendency: $E_{Alg/Car\text{-}100/00}$ (2.3 kcal mol^{-1}) = $E_{Alg/Car\text{-}95/05}$ (2.3 kcal mol^{-1}) = $E_{Alg/Car\text{-}80/20}$ (2.3 kcal mol^{-1}) > $E_{Alg/Car\text{-}90/10}$ (2.0 kcal mol^{-1}). These values are similar to those found for the activation energy of the conductivity of polysulfone membranes [42] which are in the range 2.8–3.2 kcal mol^{-1}, Nafion® 117 membranes (3.2 kcal mol^{-1}) and Nafion-reinforced membranes [43].

In Fig. 11 we represent the variation of the conductivity with the percentage of carrageenan in samples for 30, 50, 70 and 90 °C, respectively. In all the temperatures the conductivity increases with carrageenan content. An explanation of this behavior is assumed to be due to the increment of the water uptake and IEC of the membranes, which is influenced by the amount of carrageenan incorporated to the matrix of the alginate.

The transport mechanism of the proton through the membranes can be produced by Grotthus hopping mechanism or occurs in a vehicular manner, where H_3O^+ can migrate as a whole, or with a combination of both mechanisms. This is still, at the present time, a matter of discussion in the scientific literature [44]. Neglecting ion–ion interactions and convection flux, the proton flux j_+ in acidic membranes equilibrated with distilled water, under an electric field, can be expressed as $j_+ = -c_+u_+(\mathrm{d}/\mathrm{d}x)$, where c_+ is the

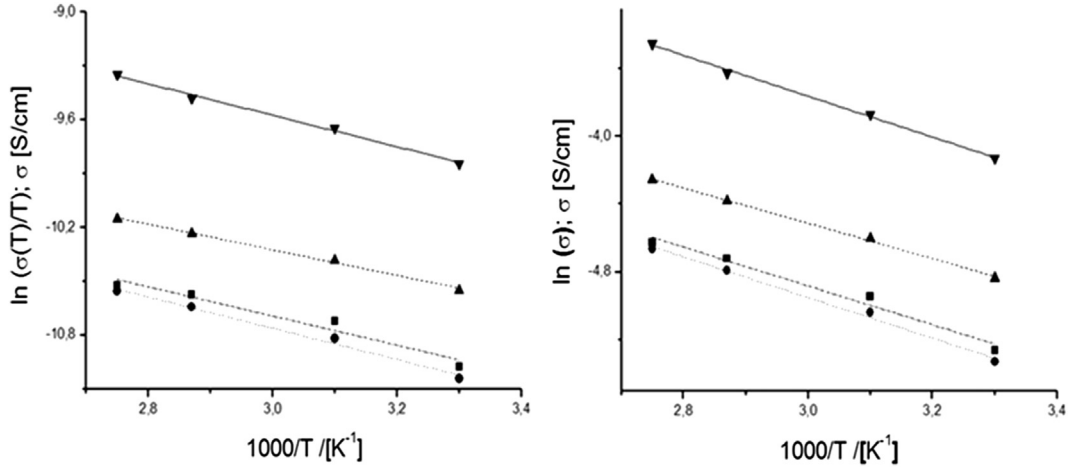

Fig. 10. Arrhenius plot for the Alg/Car membranes showing the dependence of σ/T (left) and σ (right) vs. temperature. Alg/Car 100/00 (■), Alg/Car 95/05 (●), Alg/Car 90/10 (▲), Alg/Car 80/20 (▼).

proton concentration. For cation-exchange membranes in the acid form and equilibrated with distilled water, the concentration of protons into the membrane can be considered equal to the ionic exchange capacity (c_+ = IEC of the membrane, assuming zero the concentration of the co-ion), F is the Faraday's constant, u_+ is the proton velocity (i.e. F/χ, where F is the Faraday's constant and χ the friction coefficient) and $d\psi/dx$ is the driving force. In the steady state, the friction force and the driving force per mol of proton should be equal, and taking into account the Einstein relation for the proton friction coefficient ($\chi = RT/D_+$) and the Ohm's law, the following equation which relates the conductivity and the diffusion coefficient can be obtained

$$\sigma = -\frac{i}{d\psi/dx} = \frac{c_+ F D_+}{RT} \quad (4)$$

where R is the universal gas constant, T the absolute temperature, i the current density and D_+ the proton diffusion coefficient. Table 6 shows the proton diffusion coefficients obtained at different temperatures using the eq. (4) together with the values of conductivity measured through Bode diagram and IEC. The results show that changes in the diffusion coefficient induced by changes in the IEC are relatively small. The values of diffusion coefficients found are quite close to those found in Nafion® 117 [45], and Perfluorinated nanocomposite membranes modified by polyaniline [46], but in this case our membranes had lower IEC and higher water uptake.

Values of water diffusion coefficients in Nafion® 117 measured from pulsed gradient spin-eco NMR [47] are very similar to those measured in this work for protons (see Table 6). From this we can infer that the proton diffuses by an identical mechanism than water, indicating that the proton moves as H_3O^+. This reasoning explains, for example, that the diffusion coefficient of protons in the Alg/Car 90/10 membrane varies from 2.6×10^{-6} cm^2 s^{-1} at 30 °C to 5.5×10^{-6} cm^2 s^{-1} at 90 °C.

When fuel cell data are not available, prediction of the fuel cell performance is often made using the so-called characteristic number of a specific membrane, defined by the ratio of the proton conductivity of the membrane to its methanol permeability [48,49], $\beta = \sigma/P$. Table 6 shows the values obtained for our membranes. The evaluation of this parameter is important because it is independent of the membrane thickness. A close inspection of this table shows that this number increases with the carrageenan content as the increase in conductivity follows the same trend. As mentioned above, this is influenced by the values of the water uptake and IEC increasing when the carrageenan content increases. However, for Alg/Car 100/00 membranes this parameter is about five times greater. This may be due to the low water uptake, which is in close connection with the methanol permeability. In comparison with Nafion®117 membranes this parameter is about 15 times smaller. As a conclusion, the value obtained for β predicts that Nafion®117 membrane will perform better than Alg/Car 100/00 and Alg/Car membranes at 2 M methanol concentration.

Fig. 12 shows the polarization curves for the MEAs prepared with a composite Alg/Car 80/20 membrane of 150 μm, when the DMFC is operating at 50, 70 and 90 °C with a methanol feed concentration of 2 M.

The open circuit voltage (OCV) of the cell usually does not reach the theoretical value of the overall reversible cathode and anode potential at the given temperature and pressure. The reduction of the OCV from the theoretical voltage has been attributed to the penetration of the fuel across the membrane, and thus, these values are an indicator of the degree of methanol crossover by diffusion and the catalyst efficiency [50,51].

The OCV values of our composite membrane, 610, 615 and 625 mV, are higher than the OCV for Nafion®, 0.596 V, but similar to

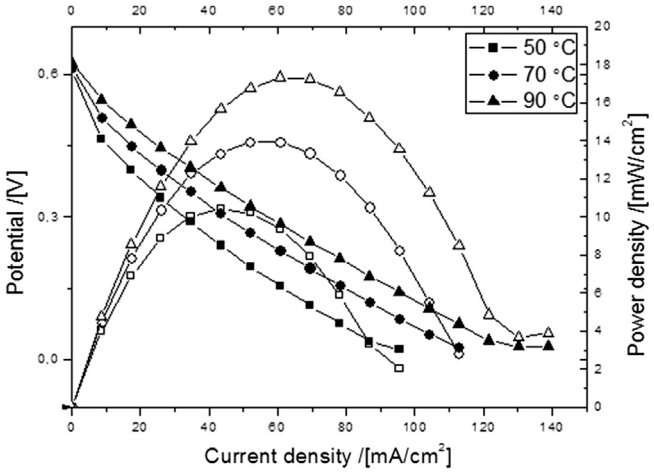

Fig. 12. *I–V* curves for DMFC experiments at 50, 70 and 90 °C and 2 M methanol concentration for Alg/Car 80/20 composite membranes. Filled symbol is used for potential and open symbol for power density.

those found in composite Nafion/PVA membranes [24]. This is corroborated by the measurements carried out by the authors in which the Nafion/PVA membranes showed a reduction of an order of magnitude in methanol permeability at 70 °C ($P \approx 4.55 \times 10^{-7}$ cm^2 s^{-1}) in comparison to commercial Nafion N117 membranes ($P \approx 4.36 \times 10^{-6}$ cm^2 s^{-1}) [23].

Although the proton conductivity of the composite membrane at these conditions is between 0.020 and 0.032 S cm^{-1}, depending on the temperature, this value is quite similar than the one measured for the pristine Nafion®, 0.032 S cm^{-1}. The resistance found in the ohmic region of the *I–V* curve (linear behavior after $i > 40$ mA cm^{-2}) is about 0.5–0.7 Ω for the Alg/Car 80/20 membrane and 0.074 Ω for the Nafion®, just one order of magnitude of difference. The reason for this much shorter difference in the ohmic resistance exhibited by the MEAs under real DMFC operation can be explained again by the fact that the composite Alg/Car membrane accomplishes a lower methanol crossover, and thus, cathode losses caused by the methanol can be smaller in the case of the composite membrane. For the Nafion® membrane, the higher proton conductivity is almost counterbalanced also by the larger methanol crossover. The maximum power densities for the MEA with the Alg/Car membrane are 10.4, 13.9 and 17.3 mW m^{-2} at 50, 70 and 90 °C, respectively.

While in the literature one can find several papers reporting the performance of pristine Nafion®, composites of Nafion® and impregnated membranes, the results cannot always be easily compared with each other since the experimental conditions can differ. For example, the results of polarization curves and power density obtained in this paper have better performance that those found for hybrid membranes based on salts of heteropolyacid, zirconium phosphate and polyvinyl alcohol (PVA–ZrP–Cs_1STA and PVA–ZrP–Cs_2STA) [51], for which, at room temperature, the power density reaches values of 2 and 6 mW cm^{-1} [2] for PVA–ZrP–Cs_1STA and PVA–ZrP–Cs_2STA hybrid membranes, respectively, working with a feed of 4 M methanol and similar conditions for the cathode, using oxygen from the surrounding air being diffused into the cathode catalyst layer.

5. Conclusions

New composite membranes of alginate, carrageenan and its mixtures have been developed from pure solutions. Alg/Car membranes, have a ductile behavior associated to this kind of bio-

polymers in comparison with other membranes used as polyelectrolyte membranes. The composite membranes have a loss of mechanical stability by the incorporation of carrageenan into the alginate matrix. A low concentration of carrageenan has a weak thermoprotective effect, which slightly delays both the T_g and T_m of the prepared membranes. The methanol permeability of the Alg/Car membranes increases with the carrageenan content. The values obtained are quite similar to the ones found for pristine Nafion® ($P \approx 2.19 \times 10^{-6}$ cm^2 s^{-1}).

The conductivity of the membranes increases with temperature following an Arrhenius behavior, with activation energies varying in the range of 2–2.3 kcal mol^{-1} for all membranes studied, independently of the amount of carrageenan. The conductivity increases when the percentage of carrageenan increases. In this sense, a 3.2 fold increase in conductivity can be achieved with Alg/Car membranes with respect to the pristine alginate membranes.

The proton diffusion coefficients obtained at different temperatures show that parameter does not significantly change with the IEC. The values found are quite close to the one found in Nafion® 117 and Perfluorinated nanocomposite membranes modified by polyaniline, and quite similar to the values found for water diffusion coefficients in Nafion® 117. Accordingly, we can infer that the proton transport follows an identical mechanism than water transport, indicating that the proton moves as H_3O^+. This reasoning explains, for example, that the diffusion coefficient of protons in Alg/Car 90/10 membranes varies from 2.59×10^{-6} cm^2 s^{-1} at 30 °C to 5.54×10^{-6} cm^2 s^{-1} at 90 °C.

Polarization curves for the MEAs prepared with a composite Alg/Car shows that the OCV values of our composite membrane are higher than the OCV for Nafion®, and the maximum power densities are 10.4, 13.9 and 17.3 mW cm^{-2} at 50, 70 and 90 °C, respectively, better performance that those found for hybrid membranes based on salts of heteropolyacid, zirconium phosphate and polyvinyl alcohol (PVA–ZrP–Cs_1STA and PVA–ZrP–Cs_2STA).

Acknowledgments

This research has been supported by the ENE/2011-24761 project, granted by the Ministerio de Ciencia e Innovación, Spain, and grants from ANPCyT, Universidad Nacional de San Luis, CONICET, Argentina. Sergio David Pasini Cabello thanks Erasmus Mundus Program for a EUROTANGO 2 fellowship at the Universidad Politécnica de Valencia (UPV).

References

[1] A.J. Appleby, F.R. Foulkes, Fuel Cell Handbook, Van Nostrand Reinhold, New York, 1989.
[2] F. Barbir, PEM Fuel Cells: Theory and Practice, Academic Press, New York, 2005.
[3] M. Rikukawa, K. Sanui, Prog. Polym. Sci. 25 (2000) 1463–1502.
[4] M.A. Hickner, H. Ghassemi, Y.S. Kim, B.R. Einsla, J.E. McGrath, Chem. Rev. 104 (2004) 4587–4612.
[5] J. Pang, H. Zhang, X. Li, Z. Jiang, Macromolecules 40 (2007) 9435–9442.
[6] Y. Yang, S. Holdcroft, Fuel Cells 5 (2005) 171–186.
[7] F. Debeaufort, J.A. Quezada-Gallo, A. Voilley, Crit. Rev. Food Sci. 38 (4) (1998) 299–313.
[8] Weikang Yuan, Hong Wu, Bin Zheng, Xiaohong Zheng, Zhongyi Jiang, Xiaopeng Hao, Baoyi Wang, J. Power Sources 172 (2007) 604–612.
[9] Jia Ma, Yogeshwar Sahai, Carbohydr. Polym. 92 (2013) 955–975.
[10] Fadime Göktepe, Sevim Ünügür Çelik, Ayhan Bozkurt, J. Non-Crystalline Solids 354 (2008) 3637–3642.
[11] Zhongyi Jiang, Xiaohong Zheng, Hong Wu, Jingtao Wang, Yabo Wang, J. Power Sources 180 (2008) 143–153.
[12] O. Smidsrød, Faraday Discuss. Chem. Soc. 57 (1974) 263–274.
[13] V. Langendorff, G. Cuvelier, C. Michon, B. Launay, A. Parker, C.G. De Kruif, Food Hydrocolloids 14 (2000) 273–280.
[14] M.S. Lizarraga, D. De Piante Vicin, R. González, A. Rubiolo, L.G. Santiago, Food Hydrocolloids 20 (5) (2006) 740–748.
[15] C.K. Yeom, K.H. Lee, J. Appl. Polym. Sci. 67 (1998) 209–219.
[16] A.M. Sajjan, B.K. Jeevan Kumar, A.A. Kittur, M.Y. Kariduraganavar, J. Memb. Sci. 425–426 (2013) 77–88.
[17] M. Saraswathi, K. Madhusudhan Rao, M.N. Prabhakar, C.V. Prasad, K. Sudakar, Desalination 269 (1–3) (2011) 177–183.
[18] Anandrao R. Kulkarni, Kumaresh S. Soppimath, Tejraj M. Aminabhavi, Pharm. Acta Helv. 74 (1999) 29–36.
[19] Anandrao R. Kulkarnia, Kumaresh S. Soppimatha, Tejraj M. Aminabhavi, Ashok M. Dave, Mahesh H. Mehta, J. Control. Release 63 (2000) 97–105.
[20] J.B. Xu, J.P. Bartley, R.A. Johnson, J. Memb. Sci. 218 (2003) 131–146.
[21] Asif Mahmooda, Saira Bano, Sang-Gyun Kim, Kew-Ho Lee, J. Memb. Sci. 415–416 (2012) 360–367.
[22] A. Mokrini, M.A. Huneault, J. Power Sources 154 (2006) 51.
[23] Sergio Mollá, Vicente Compañ, J. Power Sources 196 (2011) 2699–2708.
[24] T.S. Pathak, J.-H. Yun, S.-J. Lee, D.-J. Baek, K.-J. Paeng, Carbohydr. Polym. 78 (2009) 717–724.
[25] C.O. Illanes, E. Quiroga, J.E. Cami, N.A. Ochoa, Biochem. Eng. J. 70 (2013) 23–28.
[26] J. Yang, W. He, Int. J. Biol. Macromol. 50 (2012) 428–431.
[27] S.N. Pawar, K.J. Edgar, Carbohydr. Polym. 98 (2013) 1288–1296.
[28] Sergio Mollá, Vicente Compañ, J. Memb. Sci. 372 (2011) 191–200.
[29] S. Mollá, V. Compañ, S.L. Lafuente, J. Prats, Fuel Cells 11 (2011) 897–906.
[30] G. Raju, Dielectrics in Electric Fields, CRC Press, 2003.
[31] A. Munar, A. Andrio, R. Iserte, V. Compañ, J. Non-Crystalline Solids 357 (2011) 3064–3069.
[32] Robert J. Klein, Shihai Zhang, Shichen Dou, Brad H. Jones, Ralph H. Colby, James Runt, J. Chem. Phys. 124 (2006) 144903.
[33] R. Coelho, Rev. Phys. Appl. 18 (1983) 137.
[34] J.R. MacDonald, Phys. Rev. 92 (1953).
[35] K.W. Wagner, Arch. Electrochem. 2 (1914) 371.
[36] K.W. Wagner, Arch. Electrochem. 3 (1914) 67.
[37] R.W. Sillars, Proc. Inst. Electr. Eng. 80 (1937) 378.
[38] E. Barsoukov, J.R. MacDonald, Impedance Spectroscopy: Theory, Experiment and Application (Chapter 2), pp. 87–88, Wiley-Interscience, Chichester, 2005.
[39] S.J. Paddison, Ann. Rev. Mat. Res. 33 (2003) 289.
[40] S.J. Paddison, K.D. Kruer, J. Mater. Phys. Chem. Chem. Phys. 8 (2006) 4530.
[41] J. Pozuelo, E. Riande, E. Saiz, V. Compañ, Macromolecules 39 (2006) 8862.
[42] F.J. Fernández-Carretero, V. Compañ, E. Riande, J. Power Sources 173 (2007) 68–76.
[43] A. Kornishev, E. Spohr, in: S.J. Paddison, K.S. Promislow (Eds.), Device and Materials Modeling in PEM Fuel Cells, Springer, NY, 2009.
[44] T.E. Springer, T.A. Zawodzinski, S. Gottesfeld, J. Electrochem. Soc. 138 (1991) 23.
[45] A. Munar, K. Suarez, O. Solorza, N.P. Berezina, V. Compañ, J. Electrochem. Soc. 157 (2010) B1186–B1194.
[46] T.A. Zawoddzinski, M. Neeman, I.O. Sillerud, S. Gottesfeld, J. Phys. Chem. 95 (1991) 6040–6044.
[47] M.M. Nasef, N.A. Zubir, A.F. Ismail, K.Z.M. Dahlan, H. Saidi, M. Khayet, J. Power Sources 156 (2) (2006) 200.
[48] M.M. Nasef, N.A. Zubir, A.F. Ismail, M. Khayet, K.Z.M. Dahlan, H. Saidi, R. Rohani, T.I.S. Ngah, N.A. Sulaiman, J. Memb. Sci. 268 (1) (2006) 96.
[49] J. Larminie, A. Dicks, Fuel Cell System Explained, John Wiley & Sons Ltd, Chichester, England, 2000 (Chapter 3).
[50] T. Li-Chun Chen, Leon Yu, Hsiu-Li Lin, Sin-Hsien Yeh, J. Memb. Sci. 307 (2008) 10–20.
[51] M. Helen, B. Viswanathan, S. Srinivasa Murthy, J. Power Sources 163 (2006) 433–439.